Determining the electron scattering from interfacial Coulomb scatterers in two-dimensional transistors

Yi-Te Lee[1], Yu-Ting Huang[2,3], Shao-Pin Chiu[1], Ruey-Tay Wang[1], Takashi Taniguchi[4], Kenji Watanabe[5], Raman Sankar[6], Chi-Te Liang[3], Wei-Hua Wang[2,], Sheng-Shiuan Yeh[7,8 *], Juhn-Jong Lin[1]*

[1]Department of Electrophysics, National Yang Ming Chiao Tung University, Hsinchu 30010, Taiwan

[2]Institute of Atomic and Molecular Sciences, Academia Sinica, Taipei 106, Taiwan

[3]Department of Physics, National Taiwan University, Taipei 106, Taiwan

[4]Research Center for Materials Nanoarchitectonics, National Institute for Materials Science, 1-1 Namiki, Tsukuba 305-0044, Japan

[5]Research Center for Electronic and Optical Materials, National Institute for Materials Science, 1-1 Namiki, Tsukuba 305-0044, Japan

[6]Institute of Physics, Academia Sinica, Taipei 106, Taiwan

[7]Center for Emergent Functional Matter Science, National Yang Ming Chiao Tung University, Hsinchu 300, Taiwan

[8]International College of Semiconductor Technology, National Yang Ming Chiao Tung University, Hsinchu 30010, Taiwan

ABSTRACT

Two-dimensional (2D) transistors are promising for potential applications in next-generation semiconductor chips. Owing to the atomically thin thickness of 2D materials, the carrier scattering from interfacial Coulomb scatterers greatly suppresses the carrier mobility and hampers transistor performance. However, a feasible method to quantitatively determine relevant Coulomb scattering parameters from interfacial long-range scatterers is largely lacking. Here, we demonstrate a method to determine the Coulomb scattering strength and the density of Coulomb scattering centers in InSe transistors by comprehensively analyzing low-frequency noise and transport characteristics. Moreover, the relative contribution from long-range and short-range scattering in the InSe transistors can be distinguished. This method is employed to InSe transistors consisting of various interfaces as a model system, revealing profound effects of different scattering sources on the transport characteristics and the low-frequency noise. Quantitatively accessing the scattering parameters of 2D transistors provides valuable insight into engineering the interfaces of a wide spectrum of ultrathin-body transistors for high-performance electronics.

KEYWORDS: electron scattering, 2D materials, Coulomb scattering strength, low-frequency noise, indium selenide, interfacial Coulomb scatterers, 2D transistors

MANUSCRIPT TEXT

Introduction

Ultrathin-body field-effect transistors (FETs), including silicon-on-insulator (SOI)-FETs and Fin-FETs, exhibit a small gate screening length and have effectively facilitated the continuation of miniaturization to sub-10-nm technology.[1] To achieve shorter gate lengths, alternative technologies to further reduce the channel thickness are required.[1, 2] In particular, the dangling-bond-free surface and atomic-scale thickness of two-dimensional (2D) materials make them promising for downscaling dimensions for further miniaturization of microelectronics.[3] As the channel thickness of 2D transistors is decreased, the charge carriers are greatly scattered by the interfacial Coulomb scatterers, resulting in significant mobility degradation.[4-9] The Coulomb scattering is further intensified in 2D transistors when their channel approaches atomically thin thickness. Thus, in-depth knowledge of the Coulomb scattering parameters is crucial for designing high-performance 2D transistors. Previous studies regarding Coulomb scattering have demonstrated reduced Coulomb scattering effects and enhanced mobility via interface engineering,[10] dielectric modification, and layer thickness control.[11-13] However, a quantitative understanding of the interaction strength between charge carriers and Coulomb scatterers at interfaces, as well as the density of these long-range scattering centers, is still lacking. This knowledge gap indicates that a suitable method to directly probe these Coulomb scattering parameters is essential.

In this work, we report a unique method to determine the Coulomb scattering strength and the density of Coulomb scattering centers of 2D transistors. Our method relies on low-frequency $1/f$ noise, where f is the frequency, and electrical transport measurements without any assumptions. We apply this method to study InSe FETs with various interfaces as a model system to elucidate

the effect of Coulomb scatterers on the electrical transport and $1/f$ noise characteristics. Ohmic contact and high-quality electrical properties are realized in the InSe FETs, allowing us to explicitly study the transport characteristics of the semiconducting channel. Our method can be widely applied to various defect- and interface-engineered low-dimensional systems[14, 15] to obtain quantitative knowledge of these microscopic interfacial characteristics.

We fabricated InSe FETs with hexamethyldisilazane (HMDS)-treated SiO_2/Si, a hexagonal boron nitride (h-BN) interlayer, and a native SiO_2/Si substrate, which are designated samples A, B, and C, respectively. Figure 1a shows a schematic of our InSe FETs. The inset of Figure 1a shows an optical micrograph of a typical InSe FET with the h-BN interlayer. The topology of the InSe devices was characterized by atomic force microscopy (AFM), where an AFM image of sample B is shown in Supporting Information S1. The thickness of our InSe channels is approximately 18–30 nm. The channel thickness of InSe transistors is selected by optimizing the carrier mobility. The InSe transistors with the channel thickness of approximately 10 nm is found to exhibit high carrier density, resulting greater efficiency to screening Coulomb impurities from the adjacent interfaces. Similar thickness dependence of the performance of 2D transistors has been studied in literature.[4] On the other hand, the chosen channel thickness of InSe transistors is thin enough to allow us to probe and study the effect of carrier scatterers at the interfaces. Thee relevant parameters of the three InSe FETs studied in this work are listed in Supporting Information S2. The circuit for the electrical transport and low-frequency noise measurements is depicted in Figure 1a. Notably, the source-drain current (I_d) and frequency-dependent current noise power spectral density (PSD) $S_{I_d}(f)$ are measured simultaneously, enabling quantitative determination of each parameter and their correlation.

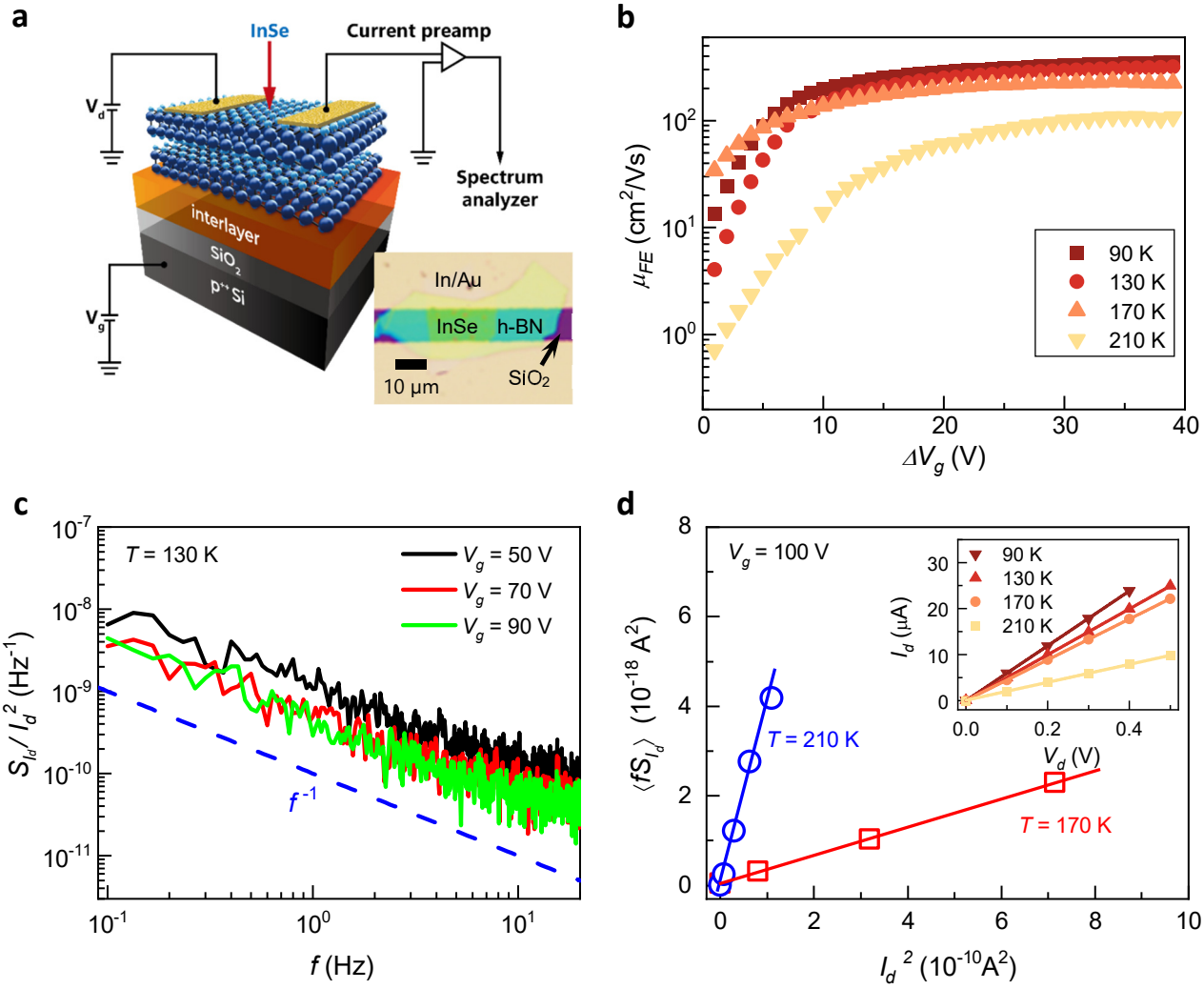

Figure 1. (a) Schematic of an InSe FET with the electrical circuit for transport characteristic and $1/f$ noise measurements. Inset: optical micrograph of a typical InSe FET with the h-BN interlayer. (b) Field-effect mobility μ_{FE} of sample A as a function of ΔV_g at four different T. (c) Normalized noise $S_{I_d}/{I_d}^2$ as a function of frequency for sample A at various V_g and T =130 K. The dashed line indicates a $1/f$ relation and is a guide to the eye. (d) $\langle f S_{I_d} \rangle$ as a function of ${I_d}^2$ for sample A at T =170 and 210 K. The solid lines are the linear fits to the data. Inset: I_d versus V_d of sample A at different T. The solid lines are the linear fits to the data.

The transfer characteristics (I_d as a function of gate voltage V_g) of samples A, B, and C reveal *n*-type behavior, as shown in Supporting Information S3. Figure 1b shows the field-effect mobility $\mu_{FE} = g_m L/C_{ox} V_d W$ of sample A as a function of $\Delta V_g = V_g - V_t$, where $g_m = dI_d/dV_g$ is the transconductance, L (W) is the length (width) of the InSe channel, C_{ox} is the specific gate capacitance, V_d is the source-drain voltage, and V_t is the threshold voltage. To reflect the transition from weak to strong inversion, we used the match-point method[16, 17] to determine the threshold voltage V_t (Supporting Information S3). For a small ΔV_g, μ_{FE} increases with ΔV_g, which can be attributed to the increased charge carrier (electron) density and stronger Coulomb screening effect as the carrier density (n) increases. μ_{FE} saturates at larger ΔV_g when the Coulomb scattering rate decreases and is overtaken by short-range scattering and electron-phonon scattering, which are not affected by the electron screening effect. μ_{FE} increases with decreasing temperature (T) for $\Delta V_g >$ 7 V, validating the intrinsic behavior of InSe at high n, which is consistent with our previous observation.[18]

Figure 1c shows the normalized noise $S_{I_d}/{I_d}^2$ as a function of frequency for sample A at different V_g and T =130 K. S_{I_d} exhibits a power law $S_{I_d} \propto f^{-\beta}$, with $\beta \approx 1.0 \pm 0.1$ in the range of $f = 0.06 - 10$ Hz. The noise data for all InSe FETs at different T show the same $1/f$ behavior. All measured S_{I_d} values are larger than the background noise by at least one order of magnitude to ensure reliable noise data from the InSe FETs instead of from extrinsic sources. The background noise in our system mostly originates from the Johnson-Nyquist noise and the noise of the current preamplifier.[19] We then calculated the average $\langle f S_{I_d} \rangle$, where $\langle f S_{I_d} \rangle = \left(\sum_{i=1}^{N} f_i S_{I_d,i}\right)/N$,[20] with i and N denoting the index and number of discrete data points of the measured $S_{I_d}(f)$, respectively. Figure 1d shows $\langle f S_{I_d} \rangle$ as a function of ${I_d}^2$ for sample A at T =170 and 210 K, indicating that

$\langle fS_{I_d} \rangle \propto {I_d}^2$. Moreover, the inset of Figure 1d shows the output curve, indicating ohmic behavior $I_d = V_d/R$ for T ranging from 90 to 210 K.[18] Consequently, the resistance fluctuations δR of our InSe FETs lead to current fluctuations $\delta I_d = (-\delta R/R) I_d$ with an applied V_d, yielding $S_{I_d} \propto {I_d}^2$ when considering the definition $S_{I_d} \propto (\delta I_d)^2$. Therefore, the observed linear relation of $\langle fS_{I_d} \rangle$ as a function of ${I_d}^2$ confirms that (i) our InSe FETs exhibit ohmic behavior, (ii) the noise originates from intrinsic resistance fluctuations,[21] and (iii) no extra resistance fluctuations are activated by the bias voltage.

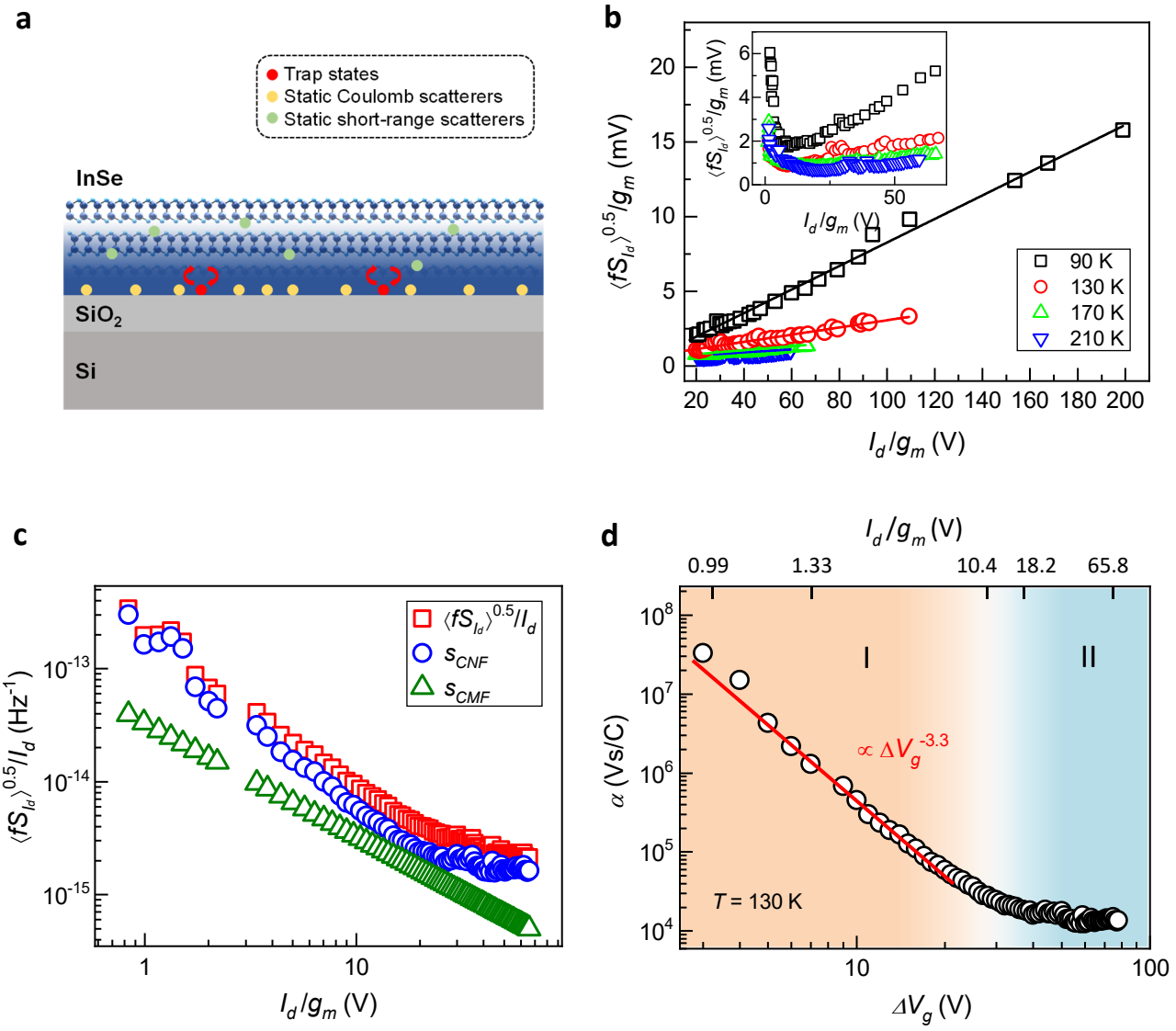

Figure 2. (a) Schematic showing the trap states, static Coulomb scatterers, and short-range scatterers in an InSe FET. The blue gradient color represents the electron density, signifying a higher electron density near the Si back gate. (b) $\langle fS_{I_d}\rangle^{1/2}/g_m$ as a function of I_d/g_m for sample A at different T. Inset: $\langle fS_{I_d}\rangle^{1/2}/g_m$ as a function of I_d/g_m for a small I_d/g_m range to show the large variation in $\langle fS_{I_d}\rangle^{1/2}/g_m$. (c) Comparison of $\left(fS_{I_d}\right)^{1/2}/I_d$, s_{CNF} and s_{CMF} as a function of I_d/g_m for sample A. (d) Extracted α as a function of ΔV_g for sample A at 130 K in a double logarithmic plot. The corresponding I_d/g_m values are indicated on the top x-axis. The solid line is a fit to the power law dependence $\alpha \propto \Delta {V_g}^{-\gamma}$.

We now discuss a method to quantitatively determine the strength of carrier scattering from interfacial Coulomb scatterers (α) and the area density of interfacial trap states (i.e., surface traps) at the Fermi energy (n_{st}). Here, α is defined as ${\mu_{C,st}}^{-1} = \alpha e n_{st}$,[22, 23] where e is the electronic charge, n_{st} is the area density of trapped charges at interfaces, and $\mu_{C,st}$ is the mobility limited by these traps. The Coulomb scattering strength α is proportional to the scattering rate of carriers from unit Coulomb scatterers, which is derived by using Fermi's golden rule. It is assumed that α is an average Coulomb scattering strength for interfacial Coulomb scatterers, thus the total scattering rate of carriers is proportional to αn_{st} based on the Matthiessen's rule. To derive α from the noise analysis, we employed the carrier number fluctuation–correlated mobility fluctuation (CNF-CMF) model,[22, 23] which has been applied to understand the low-frequency resistance noise in 2D semiconductor devices.[24-28] Neither Hooge mobility fluctuations[29, 30] nor carrier number fluctuations[31, 32] are applicable to the low-frequency noise in our InSe FETs (Supporting Information S4), suggesting the validity of the CNF-CMF mechanism. The schematic in Figure 2a

depicts major charge scattering sources, including trap states, static Coulomb, and short-range scatterers. The trapping/detrapping processes of charge carriers cause not only carrier number fluctuations but also correlated mobility fluctuations. Under an applied V_d, both the carrier number and correlated mobility fluctuations contribute to the fluctuations in I_d. Assuming that the trapping/detrapping processes of charge carriers are governed by the quantum tunneling process, the normalized current noise PSD can be written as[33]

$$\frac{S_{I_d}}{{I_d}^2} = S_{V_{fb}}\left(1 + \alpha\mu_{eff}C_{ox}\frac{I_d}{g_m}\right)^2\frac{{g_m}^2}{{I_d}^2}, \quad (1)$$

where $S_{V_{fb}} = e^2k_BTN_{st}/LW{C_{ox}}^2f$ is the PSD of the flat-band voltage noise, and k_B is Boltzmann's constant. The first and second terms in parentheses on the right-hand side correspond to CNF and CMF terms, respectively.

We now quantitatively evaluate the α and N_{st} values in InSe FETs by employing the CNF-CMF model. For comparison with experimental data, we rewrite Eq. (1) as $\langle fS_{I_d}\rangle^{1/2}/g_m = \left(fS_{V_{fb}}\right)^{1/2}\left(1 + \alpha\mu_{eff}C_{ox}\,I_d/g_m\right)$, designated as Eq. (1A). Figure 2b shows $\langle fS_{I_d}\rangle^{1/2}/g_m$ as a function of I_d/g_m for sample A. For $I_d/g_m > 10$ V, $\langle fS_{I_d}\rangle^{1/2}/g_m$ linearly increases with I_d/g_m, suggesting that $\alpha\mu_{eff}$ is a constant of I_d/g_m in this regime. Importantly, the linear dependence of $\langle fS_{I_d}\rangle^{1/2}/g_m$ on I_d/g_m at high I_d/g_m allows us to determine the N_{st} value, which can be extracted from the intercept $\left(fS_{V_{fb}}\right)^{1/2} = \left(e^2k_BTN_{st}/LW{C_{ox}}^2\right)^{1/2}$ of the linear fitting. Moreover, we can rewrite Eq. (1) to obtain the square root of the normalized measured noise PSD,

$$\langle fS_{I_d}\rangle^{\frac{1}{2}}/I_d = \left(fS_{V_{fb}}\right)^{1/2}(I_d/g_m)^{-1} + \left(fS_{V_{fb}}\right)^{1/2}\alpha\mu_{eff}C_{ox} \equiv s_{CNF} + s_{CMF}, \quad (2)$$

where $s_{CNF} = \left(fS_{V_{fb}}\right)^{1/2} (I_d/g_m)^{-1}$ and $s_{CMF} = \left(fS_{V_{fb}}\right)^{1/2} \alpha\mu_{eff}C_{ox}$ (2A) are the noise caused by CNFs and CMFs, respectively. N_{st}, and thus s_{CNF}, can be extracted from the data, followed by the determination of s_{CMF} based on $s_{CMF} = \langle fS_{I_d}\rangle^{\frac{1}{2}}/I_d - s_{CNF}$. Figure 2c compares $\langle fS_{I_d}\rangle^{\frac{1}{2}}/I_d$, s_{CNF} and s_{CMF} as a function of I_d/g_m, indicating that the s_{CMF} noise significantly contributes to the measured noise $\langle fS_{I_d}\rangle^{\frac{1}{2}}/I_d$. We can now extract the Coulomb scattering strength α according to Eq. 2A, which is one of the central goals of this work. The determination of both α and N_{st} in this method does not require any assumptions, as the remaining parameters can be determined from the $1/f$ noise and transport measurements.

Figure 2d shows the extracted α as a function of ΔV_g for sample A at T =130 K in a double logarithmic plot, exhibiting a monotonically decreasing trend with increasing ΔV_g. The ΔV_g dependence of α can be characterized into two distinct regimes: At low ΔV_g ($\Delta V_g < 30$ V, regime I), α rapidly decreases with ΔV_g. At high ΔV_g ($\Delta V_g > 30$ V, regime II), the ΔV_g dependence of α becomes relatively weak. Notably, α varies by four orders of magnitude with ΔV_g ranging from ≈ 1 V to ≈ 80 V. In regime I, the carrier density increases with increasing V_g, leading to enhanced Coulomb screening and a rapid decrease in α with V_g.[34] α follows the power law $\alpha \propto {\Delta V_g}^{-3.3}$ for 3 V$< \Delta V_g <$ 30 V. In previous reports, a power law of $\alpha \propto n^{-\nu}$ was assumed to describe the carrier density dependence of α,[24-28] where $\nu \approx$ 1.2–1.6 and $\nu \approx$ 0.9 were reported for $MoTe_2$[24] and WS_2 devices,[25] respectively. The comparatively large exponent of 3.3 indicates a very strong screening effect, which may be qualitatively understood in terms of a significantly induced electron density in InSe[35] compared with other 2D semiconductors. To further discuss the rapid decrease in α with increasing $\triangle V_g$, we plot $\langle fS_{I_d}\rangle^{1/2}/g_m$ in the small I_d/g_m range (inset of

Figure 2b). α is inferred to drastically decrease with increasing I_d/g_m to overtake the trend of μ_{FE} (Supporting Information S5), further supporting the very large ΔV_g dependence in regime I. In regime II, α weakly decreases with ΔV_g compared with the trend in regime I and gradually saturates, which may be ascribed to saturation of the screening effect from Coulomb scatters in this regime.

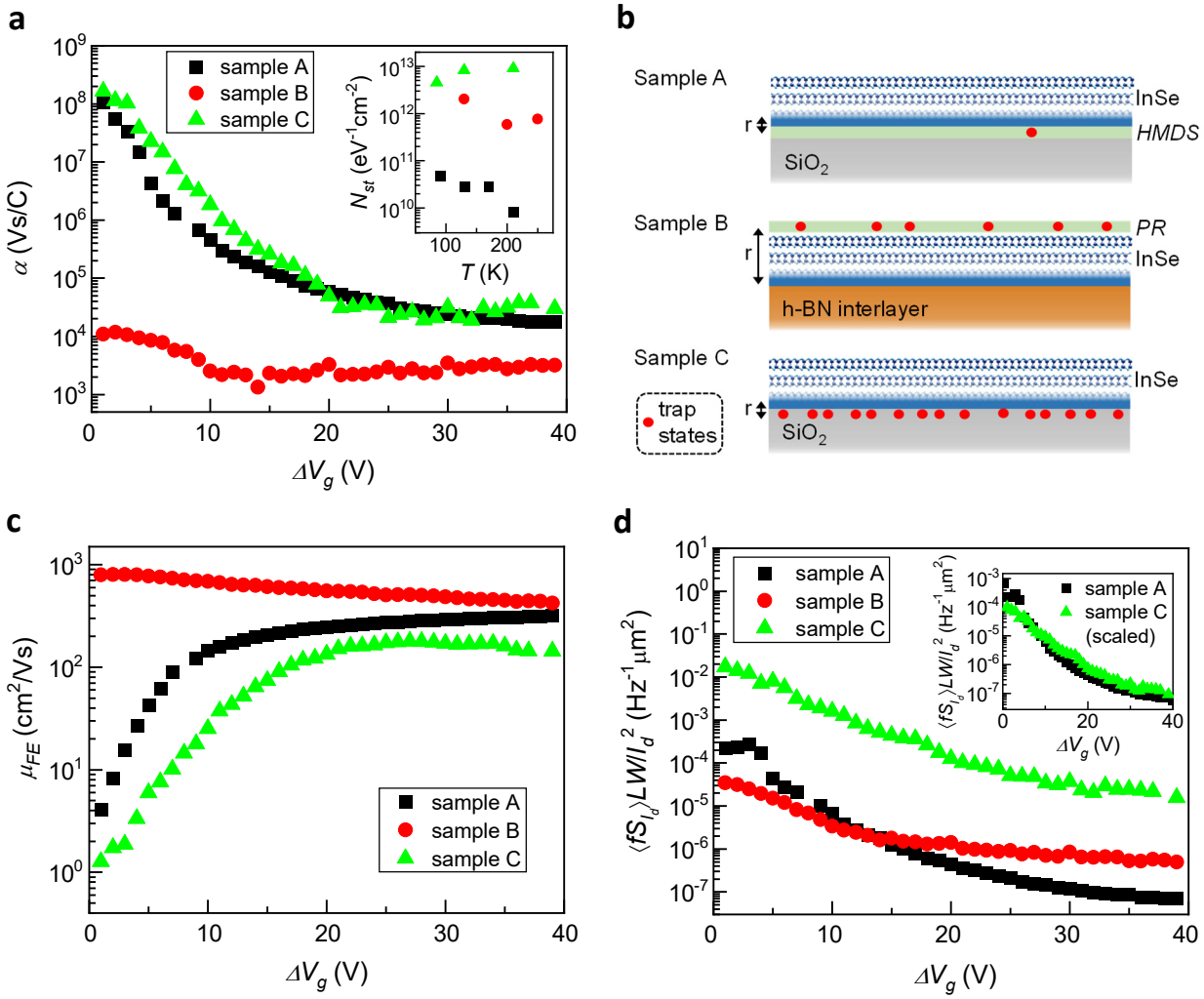

Figure 3. (a) Comparison of α as a function of ΔV_g for samples A, B, and C at T =130 K. Sample B exhibits very small Coulomb scattering in InSe FETs with the h-BN interlayer. Inset: N_{st} as a function of T for samples A, B, and C. (b) Schematics illustrating the distribution of the trap states

and their relative distance r to the charge carriers in the InSe channel for samples A, B, and C. The blue gradient color represents the electron density, signifying a higher electron density near the Si back gate. (c) Comparison of the field-effect mobility μ_{FE} as a function of ΔV_g for samples A, B, and C at $T = 130$ K. (d) Area-normalized noise PSD $\langle fS_{I_d} \rangle LW/{I_d}^2$ as a function of ΔV_g for samples A, B, and C at $T = 130$ K. Inset: comparison of the $\langle fS_{I_d} \rangle LW/{I_d}^2$ of sample A and the scaled noise PSD of sample C at $T = 130$ K.

Having established the method to determine α and N_{st}, we now apply it to elucidate the effect of the interfacial properties of the InSe FETs by comparing the Coulomb scattering parameters of samples A, B, and C. Figure 3a compares the measured α values for samples A, B, and C at 130 K, which all exhibit similar behavior as those for sample A, as discussed in Figure 2d. The α values for samples A and C are comparable for the range of all measured ΔV_g. α characterizes the Coulomb scattering rate, and thus, $\alpha \propto {V_C}^2$ according to Fermi's golden rule, where V_C is the Coulomb potential that depends on the carrier density and the distance between the charge carrier and the interfacial impurity (r). For samples A and C, the major trap sites reside at the InSe/SiO_2 interface, as depicted in Figure 3b; thus, V_C is similar in the two samples. Therefore, the ΔV_g dependences of α for these two samples being comparable is reasonable.

Remarkably, the α determined for sample B is smaller than that for samples A and C by four orders of magnitude at $\Delta V_g = 0$, indicating very small Coulomb scattering for the InSe FETs with the h-BN interlayer. As depicted in Figure 3b, the distance r for samples A and C can be assumed to be on the order of 0.1 nm by noting that the interaction between the InSe channel and the substrate is governed by the van der Waal force[36] and that the dominant carriers are induced adjacent to the InSe/SiO_2 interface under an applied V_g.[37] In contrast, while the bottom InSe

interface of sample B is pristine, polydimethylsiloxane (PDMS) residue can be present on the top InSe interface,[5] suggesting that the r in sample B can be approximated by the thickness of the InSe channel, which is on the order of 10 nm (Supporting Information S1). At $\Delta V_g = 0$, $n \approx 0$, and the Coulomb screening effect is negligible; the Coulomb potential is $V_C \propto {\varepsilon_r}^{-1} r^{-1}$, where ε_r is the dielectric constant. For sample B, r is larger than that for samples A and C by two orders of magnitude. Therefore, we can estimate that the α for sample B is smaller than that for samples A and C by four orders of magnitude, which is in reasonable agreement with the experimental data. Importantly, clean InSe/h-BN interfaces adjacent to the dominant carriers are achieved, which has a profound effect on reducing α. Furthermore, the ΔV_g dependence of α at low ΔV_g of sample B is much weaker than that of samples A and C. Considering that the n near the top InSe interface is low and that the Coulomb screening of the scatterers at this interface is much weaker, α likely exhibits a small variation with ΔV_g.

The inset of Figure 3a shows N_{st} as a function of T for samples A, B, and C. The average N_{st} of sample A (HMDS-treated SiO_2) is on the order of 10^{10} eV^{-1} cm^{-2} and is smaller than that of sample C (intrinsic SiO_2) by two orders of magnitude. Because the HMDS-treated SiO_2 yields a hydrophobic surface that greatly reduces the number of adsorbates,[38] the large difference in N_{st} suggests that the trap states may be attributed to the water molecules absorbed at the InSe/SiO_2 interface. This ascription of trap states is in line with previous reports for single-crystal pentacene FETs[39] and MoS_2 FETs.[40] As a comparison, a high N_{st} on the order of $10^{11} - 10^{13}$ eV^{-1} cm^{-2} was commonly observed in $MoTe_2$ and MoS_2 devices when the surface of substrates was not pretreated,[24, 26-28] indicating the importance of the hydrophobic surface treatment. The $N_{st} \sim 1 \times 10^{12}$ eV^{-1} cm^{-2} for sample B is high, which may originate from the PDMS residue on the top InSe interface.[5]

Figure 3c compares μ_{FE} as a function of ΔV_g for samples A, B, and C. The μ_{FE} of sample C increases as ΔV_g increases and saturates when $\Delta V_g > 20$ V, showing a trend similar to that for sample A, as discussed in Figure 1b. Moreover, the μ_{FE} of sample A is higher than that of sample C, which can be accounted for by a lower interfacial density of static Coulomb scatters in sample A caused by surface treatment (Supporting Information S2), considering that α is comparable in these two samples. Sample B exhibits higher μ_{FE} than samples A and C, which is consistent with the lower value of α. Interestingly, the μ_{FE} in sample B is high despite its large N_{st}, indicating the dominant role of the long-range Coulomb scattering strength α in determining μ_{FE}. The μ_{FE} of sample B monotonically decreases with ΔV_g, revealing different behavior compared with samples A and C. Because α is very small in sample B, Coulomb scattering can be overtaken by other scattering mechanisms. The atypical behavior of the μ_{FE} of sample B may be attributed to surface roughness scattering,[41] which becomes stronger with increasing number of induced carriers, resulting in μ_{FE} decreasing with increasing ΔV_g.

We now discuss the noise properties of the InSe FETs by further examining the associated N_{st} and α. Figure 3d shows the area-normalized noise PSD $\langle fS_{I_d}\rangle LW/{I_d}^2$ for samples A, B, and C. The normalized noise PSD of sample A is smaller than that of sample C by approximately two orders of magnitude. This difference can be understood by referring to Eq. (1): the α values are comparable for samples A and C, as shown in Figure 3a, while the N_{st} values in sample A are smaller than those in sample C by approximately two orders of magnitude. Additionally, we scale the normalized noise PSD of sample C by the N_{st} ratio, as shown in the inset of Figure 3d. The scaled data of sample C collapse onto those of sample A, suggesting the validity of our analysis. Therefore, the largely suppressed noise in sample A can be attributed to a great reduction in N_{st} due to the HMDS treatment. In addition, by comparing the area-normalized noise of the three

samples, the trap centers are inferred to be located at interfaces instead of in the bulk of the InSe channel (Supporting Information S6).

Finally, we discuss the density of interfacial Coulomb scatterers n_C and the mobility associated with different scattering mechanisms given that α is determined. The mobility corresponding to Coulomb scattering μ_C can be written as[22]

$$\mu_C{}^{-1} = \alpha' e n_C. \quad (3)$$

The factor α' in Eq. (3) corresponds to both static and dynamic Coulomb scatterers, while the α in Eq. (1) is only associated with the trap states. In this work, we presume that both static and dynamic Coulomb scatterers reside at the same interface, resulting in the same α value for both scattering sources, and thus, $\alpha' \approx \alpha$. The effective mobility $\mu_{eff} \approx \mu_{FE}$ and can be expressed as

$$\frac{1}{\mu_{FE}} \approx \frac{1}{\mu_{eff}} = \frac{1}{\mu_C} + \frac{1}{\mu_s} + \frac{1}{\mu_{ph}}, \quad (4)$$

where μ_s and μ_{ph} are the mobilities corresponding to short-range scattering and electron-phonon scattering, respectively. Because at low ΔV_g, where electron screening is weak, Coulomb scattering is strong and dominant,[9] we can assume $\mu_{FE}{}^{-1} \approx \mu_C{}^{-1}$ in this regime. We then estimate n_C at low ΔV_g based on Eq. (3), yielding n_C values of 1.4×10^{10} and 3.0×10^{10} cm^{-2} for samples A and C at $T = 130$ K, respectively. With the extracted n_C, we can then calculate the ΔV_g dependence of $\mu_C{}^{-1}$ based on Eq. (3). Figure 4a compares $\mu_{FE}(\Delta V_g)$ and $\mu_C(\Delta V_g)$ for sample A at 130 K. For $\Delta V_g > 5$ V, μ_{FE} increases slower and deviates from the trend of μ_C. This suppression of μ_{FE} can be qualitatively understood because when Coulomb scattering is strongly screened at higher ΔV_g, other scattering mechanisms, i.e., short-range scattering ($\mu_s{}^{-1}$) and phonon scattering ($\mu_{ph}{}^{-1}$), become dominant in the regime.

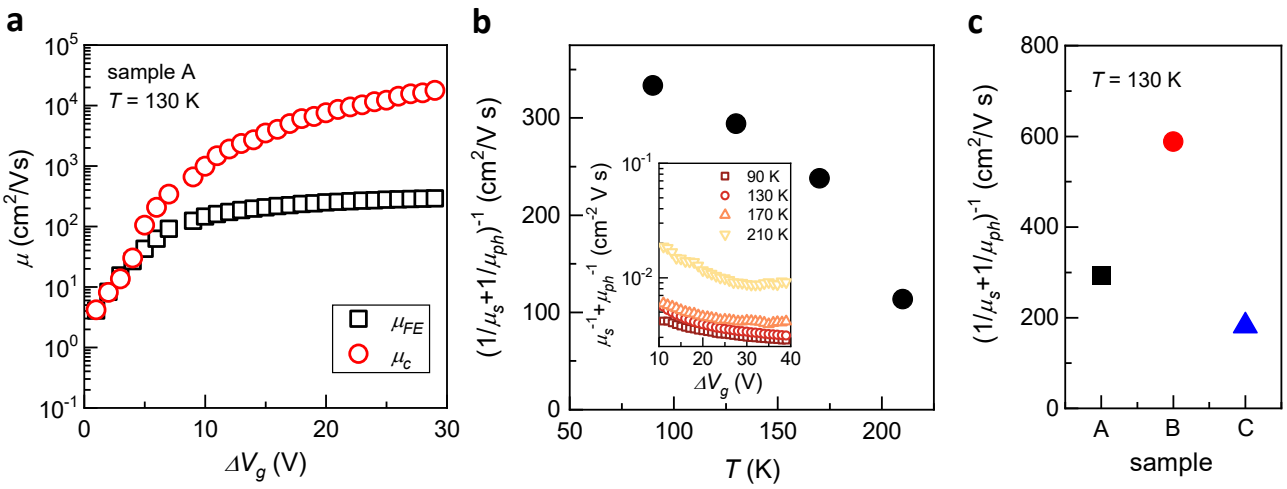

Figure 4. (a) Comparison of μ_{FE} and μ_C as a function of ΔV_g for sample A at T =130 K. The area density of interfacial Coulomb scatterers n_C is estimated in a regime dominated by Coulomb scattering. (b) T dependence of the mobility limited by the short-range and phonon scattering $\left({\mu_s}^{-1} + {\mu_{ph}}^{-1}\right)^{-1}$ of sample A at $\Delta V_g = 30$ V. Inset: plot of ${\mu_s}^{-1} + {\mu_{ph}}^{-1}$ as a function of ΔV_g at different T for sample A. (c) Comparison of $\left({\mu_s}^{-1} + {\mu_{ph}}^{-1}\right)^{-1}$ for samples A, B, and C at T =130 K. Sample B exhibits the highest mobility corresponding to the fewest short-range scattering centers at interface compared with samples A and C.

To further distinguish the contributions from different scattering mechanisms, we subtracted ${\mu_C}^{-1}$ from ${\mu_{FE}}^{-1}$ according to Eq. (4). The inset of Figure 4b plots ${\mu_s}^{-1} + {\mu_{ph}}^{-1}$ as a function of ΔV_g at various T for sample A. For a given T, ${\mu_s}^{-1} + {\mu_{ph}}^{-1}$ slightly decreases with n, which may be attributed to the screening of the remote interfacial phonon scattering at large n.[42, 43] ${\mu_s}^{-1} + {\mu_{ph}}^{-1}$ saturates for $\Delta V_g > 30$ V due to weakening electron screening. When T decreases from 210 K to 90 K, ${\mu_s}^{-1} + {\mu_{ph}}^{-1}$ decreases by a factor of approximately 5. Figure 4b plots the T

dependence of the mobility corresponding to the short-range and electron-phonon scattering $\left({\mu_s}^{-1}+{\mu_{ph}}^{-1}\right)^{-1}$ at $\triangle V_g = 30$ V. $\left({\mu_s}^{-1}+{\mu_{ph}}^{-1}\right)^{-1}$ increases with decreasing T because the electron-phonon scattering rate is suppressed. $\left({\mu_s}^{-1}+{\mu_{ph}}^{-1}\right)^{-1}$ approaches a constant value at lower T as electron-phonon scattering becomes negligible, enabling determination of the mobility for short-range scattering. Figure 4c compares the $\left({\mu_s}^{-1}+{\mu_{ph}}^{-1}\right)^{-1}$ for samples A, B, and C at 130 K. The assumption that the μ_{ph} and μ_s corresponding to the bulk short-range scatterers are comparable in these devices is reasonable, considering the same measured T and source bulk crystal. Therefore, the value of $\left({\mu_s}^{-1}+{\mu_{ph}}^{-1}\right)^{-1}$ reflects the number of short-range scatterers at the interfaces for these samples. Sample B exhibits the highest $\left({\mu_s}^{-1}+{\mu_{ph}}^{-1}\right)^{-1}$, which can be attributed to fewer short-range scattering centers at InSe/h-BN interface compared with that of InSe/SiO_2 interface.

In summary, we demonstrated a method to quantitatively extract the Coulomb and short-range scattering parameters in 2D transistors by combining the low-frequency $1/f$ noise behavior and the transfer characteristics. The extracted long-range Coulomb scattering strength of 2D transistors is found to be a nontrivial function of the carrier density, as opposed to the previous understanding of a simple power law. We applied our method to study InSe FETs with different interfaces and obtained comprehensive correlations between the relevant Coulomb scattering parameters. In particular, InSe FETs with the h-BN interlayer exhibit high mobility and low noise, which can be attributed to the clean InSe/h-BN interfaces and the very low Coulomb scattering strength measured. This method can be applied to a wide spectrum of 2D FETs with different channel materials and various interfaces as well as ultrathin-body FETs to understanding the role of Coulomb scattering. This in-depth knowledge of the Coulomb scattering strength and its key

influences on the transport characteristics and low-frequency noise properties are highly useful for tailoring the interface and developing high-performance electronics.

METHODS

2D InSe FETs fabrications. The InSe and hexagonal boron nitride (h-BN) flakes are mechanically exfoliated onto the Si substrate with a 300-nm-thick SiO_2 dielectric layer. The high-quality InSe crystals are grown by Bridgman method. The mechanical exfoliation of InSe flakes was performed in ambient condition. We then annealed the InSe samples in a furnace at 300 °C with Ar 95% and H_2 5% forming gas to remove the PDMS residues. The InSe samples were then loaded into an e-beam evaporation system in high vacuum to deposit the contact metal. To achieve clean interface, the InSe samples were kept in a vacuum of 1×10^{-8} Torr for 15 h before In/Au (3 nm/80 nm) metallic films was deposited as the electrical contacts at a base pressure of 1×10^{-7} Torr. We fabricated three types of samples with different interfaces, including hexamethyldisilazane (HMDS)-treated SiO_2, h-BN interlayer, and intrinsic SiO_2/Si substrates. For the samples with HMDS treatment, ambient adsorbates such as water molecules can be greatly reduced compared with unprocessed SiO_2 surface.[38] For the samples with an h-BN interlayer, the exfoliated InSe crystals were transferred onto h-BN flakes, which were pre-exfoliated on a SiO_2/Si substrates. Back gate voltage is applied to Si substrates to tune the carrier density in InSe.

Electrical measurements. In the measurement, all InSe devices are enclosed in a sample space of a cryostat which is immersed in liquid nitrogen. The sample space is filled with helium gas. The devices are connected by twisted-pair measurement wires to suppress the magnetically induced current noise originated from the electromagnetic fluctuations in the laboratory environment. The electrical measurement circuit for transfer characteristic (the drain current I_d as a function of gate voltage V_g) and low-frequency noise is schematically depicted in Figure 1(a) in the main text. The gate voltage V_g is applied to the heavily doped (p^{++}) Si substrate. Two sourcemeters (Keithley 6430) are used to apply the V_g and the source-drain voltage V_d. The drain current as a function of

time $I_d(t)$ is amplified and converted to voltage by the current preamplifier (Stanford Research Systems model SR570) and then measured by the dynamic spectrum analyzer (Stanford Research Systems model SR785). The SR785 probes the signal with a sampling rate of 1024 Hz and measurement time of 30 s and stored the readings in the buffers.[19] A computer fetches the data from the buffers, divide them by the gain of the SR570 and calculates the source-drain current noise power spectrum density (PSD) $S_{I_d}(f)$ using a LabVIEW program. The $S_{I_d}(f)$ and the I_d are measured simultaneously. For each V_g, the $S_{I_d}(f)$ is measured 10 times and is averaged to minimize the uncertainty of the noise. The InSe FETs were mounted in a cryostat and cooled with liquid nitrogen to study the T dependence of transport property and low-frequency noise from 300 K to 80 K. The measurement is performed in a helium atmosphere. The sample temperature is monitored with a calibrated silicon diode thermometer.

ASSOCIATED CONTENT

Supporting Information. Characterization of the InSe channel by atomic force microscopy. Comparison of the density of interfacial trap states N_{st} and area density of Coulomb impurities n_c among samples A, B, and C. Transfer characteristics for samples A, B, and C. Mechanism of the low-frequency noise in the InSe FETs. Correlation between I_d/g_m and $V_g - V_t$. Consideration of interfacial and bulk trap defects.

AUTHOR INFORMATION

Corresponding Author

*Wei-Hua Wang Tel: +886 2 2366 8208 E-mail: wwang@sinica.edu.tw

†Sheng-Shiuan Yeh Tel: +886 978 098 108 E-mail: ssyeh@nycu.edu.tw

Author Contributions

Y.T.L., W.H.W., S.S.Y., and J.J.L. conceived the experiment. Y.T.H. fabricated and characterized the InSe FETs with the assistance from W.H.W. and C.T.L. Y.T.L. and S.S.Y. performed the experimental measurements with assistance from S.P.C. and R.T.W. T.T. and K.W. synthesized the h-BN crystals. R.S. synthesized the InSe crystals. Y.T.L., W.H.W., S.S.Y., and J.J.L. analyzed and explained the data. S.S.Y., W.H.W., J.J.L., and C.T.L. wrote the manuscript. All the authors discussed the data and the manuscript.

ACKNOWLEDGMENT

This work was supported by the National Science and Technology Council (NSTC) of Taiwan through Grant Nos. 110-2112-M-A49-015 and 111-2119- M-007-005 (J.J.L.), 110-2112-M-A49-033-MY3 (S.S.Y.), 112-2119-M-002-014 (C.T.L.), and 109-2112-M-001-041-MY3 (W.H.W). R. S. acknowledges the financial support provided by the NSTC under project number 110-2112-M-001-065-MY3 and Academia Sinica for the budget of AS-iMATE-109-13. S.S.Y. is grateful to the support by Taiwan Ministry of Education through the Higher Education Sprout Project of the NYCU. K.W. and T.T. acknowledge support from the JSPS KAKENHI (Grant Numbers 20H00354, 21H05233 and 23H02052) and World Premier International Research Center Initiative (WPI), MEXT, Japan.

REFERENCES

1. Liu, Y.; Duan, X.; Shin, H.-J.; Park, S.; Huang, Y.; Duan, X., Promises and Prospects of Two-Dimensional Transistors. *Nature* **2021,** *591* (7848), 43-53.
2. Si, M. W.; Lin, Z. H.; Chen, Z. Z.; Sun, X.; Wang, H. Y.; Ye, P. D., Scaled Indium Oxide Transistors Fabricated Using Atomic Layer Deposition. *Nat Electron* **2022,** *5* (3), 164-170.
3. Desai, S. B.; Madhvapathy, S. R.; Sachid, A. B.; Llinas, J. P.; Wang, Q.; Ahn, G. H.; Pitner, G.; Kim, M. J.; Bokor, J.; Hu, C.; Wong, H.-S. P.; Javey, A., MoS_2 Transistors with 1-Nanometer Gate Lengths. *Science* **2016,** *354* (6308), 99-102.
4. Li, S.-L.; Wakabayashi, K.; Xu, Y.; Nakaharai, S.; Komatsu, K.; Li, W.-W.; Lin, Y.-F.; Aparecido-Ferreira, A.; Tsukagoshi, K., Thickness-Dependent Interfacial Coulomb Scattering in Atomically Thin Field-Effect Transistors. *Nano Lett* **2013,** *13* (8), 3546-3552.
5. Cui, X.; Lee, G.-H.; Kim, Y. D.; Arefe, G.; Huang, P. Y.; Lee, C.-H.; Chenet, D. A.; Zhang, X.; Wang, L.; Ye, F.; Pizzocchero, F.; Jessen, B. S.; Watanabe, K.; Taniguchi, T.; Muller, D. A.; Low, T.; Kim, P.; Hone, J., Multi-Terminal Transport Measurements of Mos2 Using a Van Der Waals Heterostructure Device Platform. *Nat Nanotechnol* **2015,** *10* (6), 534-540.
6. Ju, S.; Liang, B.; Zhou, J.; Pan, D.; Shi, Y.; Li, S., Coulomb Screening and Scattering in Atomically Thin Transistors across Dimensional Crossover. *Nano Lett* **2022,** *22* (16), 6671-6677.
7. Uchida, K.; Junji, K.; Shin-ichi, T. In *Experimental Study on Carrier Transport Mechanisms in Double- and Single-Gate Ultrathin-Body Mosfets - Coulomb Scattering, Volume Inversion, and /Spl Delta/T/Sub Soi/-Induced Scattering*, IEEE International Electron Devices Meeting 2003, 8-10 Dec. 2003; 2003; pp 33.5.1-33.5.4.
8. Gamiz, F.; Jiménez-Molinos, F.; Roldán, J. B.; Cartujo-Cassinello, P., Coulomb Scattering Model for Ultrathin Silicon-on-Insulator Inversion Layers. *Appl Phys Lett* **2002,** *80* (20), 3835-3837.
9. Ma, N.; Jena, D., Charge Scattering and Mobility in Atomically Thin Semiconductors. *Phys Rev X* **2014,** *4* (1), 011043.
10. Cho, K.; Pak, J.; Chung, S.; Lee, T., Recent Advances in Interface Engineering of Transition-Metal Dichalcogenides with Organic Molecules and Polymers. *Acs Nano* **2019,** *13* (9), 9713-9734.
11. Bao, W.; Cai, X.; Kim, D.; Sridhara, K.; Fuhrer, M. S., High Mobility Ambipolar Mos2 Field-Effect Transistors: Substrate and Dielectric Effects. *Appl Phys Lett* **2013,** *102* (4), 042104.
12. Radisavljevic, B.; Kis, A., Mobility Engineering and a Metal–Insulator Transition in Monolayer Mos2. *Nat Mater* **2013,** *12* (9), 815-820.
13. Feng, W.; Zheng, W.; Cao, W.; Hu, P., Back Gated Multilayer Inse Transistors with Enhanced Carrier Mobilities Via the Suppression of Carrier Scattering from a Dielectric Interface. *Adv Mater* **2014,** *26* (38), 6587-6593.
14. Ford, A. C.; Ho, J. C.; Chueh, Y.-L.; Tseng, Y.-C.; Fan, Z.; Guo, J.; Bokor, J.; Javey, A., Diameter-Dependent Electron Mobility of Inas Nanowires. *Nano Lett* **2009,** *9* (1), 360-365.
15. Konar, A.; Mathew, J.; Nayak, K.; Bajaj, M.; Pandey, R. K.; Dhara, S.; Murali, K. V. R. M.; Deshmukh, M. M., Carrier Transport in High Mobility Inas Nanowire Junctionless Transistors. *Nano Lett* **2015,** *15* (3), 1684-1690.

16. Ortiz-Conde, A.; García-Sánchez, F. J.; Muci, J.; Terán Barrios, A.; Liou, J. J.; Ho, C.-S., Revisiting Mosfet Threshold Voltage Extraction Methods. *Microelectronics Reliability* **2013,** *53* (1), 90-104.
17. Schroder, D. K., *Semiconductor Material and Device Characterization*. Wiley: 2015.
18. Huang, Y. T.; Chen, Y. H.; Ho, Y. J.; Huang, S. W.; Chang, Y. R.; Watanabe, K.; Taniguchi, T.; Chiu, H. C.; Liang, C. T.; Sankar, R.; Chou, F. C.; Chen, C. W.; Wang, W. H., High-Performance Inse Transistors with Ohmic Contact Enabled by Nonrectifying Barrier-Type Indium Electrodes. *Acs Appl Mater Inter* **2018,** *10* (39), 33450-33456.
19. Yeh, S.-S.; Chang, W.-Y.; Lin, J.-J., Probing Nanocrystalline Grain Dynamics in Nanodevices. *Science Advances* **2017,** *3* (6), e1700135.
20. Yeh, S.-S.; Gao, K. H.; Wu, T.-L.; Su, T.-K.; Lin, J.-J., Activation Energy Distribution of Dynamical Structural Defects in Ruo_2 Films. *Physical Review Applied* **2018,** *10* (3), 034004.
21. Hooge, F. N., 1/Ƒ Noise Is No Surface Effect. *Phys. Lett. A* **1969,** *29* (3), 139-140.
22. Hung, K. K.; Ko, P. K.; Hu, C.; Cheng, Y. C., A Unified Model for the Flicker Noise in Metal-Oxide-Semiconductor Field-Effect Transistors. *IEEE Transactions on Electron Devices* **1990,** *37* (3), 654-665.
23. Ghibaudo, G.; Roux, O.; Nguyen-Duc, C.; Balestra, F.; Brini, J., Improved Analysis of Low Frequency Noise in Field-Effect Mos Transistors. *phys. stat. sol. (a)* **1991,** *124* (2), 571-581.
24. Ji, H.; Joo, M.-K.; Yun, Y.; Park, J.-H.; Lee, G.; Moon, B. H.; Yi, H.; Suh, D.; Lim, S. C., Suppression of Interfacial Current Fluctuation in $Mote_2$ Transistors with Different Dielectrics. *Acs Appl Mater Inter* **2016,** *8* (29), 19092-19099.
25. Joo, M.-K.; Yun, Y.; Yun, S.; Lee, Y. H.; Suh, D., Strong Coulomb Scattering Effects on Low Frequency Noise in Monolayer Ws_2 Field-Effect Transistors. *Appl Phys Lett* **2016,** *109* (15), 153102.
26. Joo, M.-K.; Moon, B. H.; Ji, H.; Han, G. H.; Kim, H.; Lee, G.; Lim, S. C.; Suh, D.; Lee, Y. H., Understanding Coulomb Scattering Mechanism in Monolayer Mos_2 Channel in the Presence of H-Bn Buffer Layer. *Acs Appl Mater Inter* **2017,** *9* (5), 5006-5013.
27. Ji, H.; Lee, G.; Joo, M.-K.; Yun, Y.; Yi, H.; Park, J.-H.; Suh, D.; Lim, S. C., Thickness-Dependent Carrier Mobility of Ambipolar $Mote_2$: Interplay between Interface Trap and Coulomb Scattering. *Appl Phys Lett* **2017,** *110* (18), 183501.
28. Ji, H.; Joo, M.-K.; Yi, H.; Choi, H.; Gul, H. Z.; Ghimire, M. K.; Lim, S. C., Tunable Mobility in Double-Gated $Mote_2$ Field-Effect Transistor: Effect of Coulomb Screening and Trap Sites. *Acs Appl Mater Inter* **2017,** *9* (34), 29185-29192.
29. Dutta, P.; Dimon, P.; Horn, P. M., Energy Scales for Noise Processes in Metals. *Phys. Rev. Lett.* **1979,** *43* (9), 646-649.
30. Fleetwood, D. M.; Giordano, N., Direct Link between 1/*F* Noise and Defects in Metal Films. *Phys. Rev. B* **1985,** *31* (2), 1157-1160.
31. McWhorter, A. L., In *Semiconductor Surface Physics*, Kingston, R. H., Ed. University of Pennsylvania: Philadelphia, 1957.
32. Fleetwood, D. M.; Meisenheimer, T. L.; Scofield, J. H., 1/F Noise and Radiation Effects in Mos Devices. *IEEE Transactions on Electron Devices* **1994,** *41* (11), 1953-1964.
33. Ghibaudo, G.; Roux, O.; Nguyen-Duc, C.; Balestra, F.; Brini, J., Improved Analysis of Low Frequency Noise in Field-Effect Mos Transistors. *Phys. Stat. Sol. (Aphys. stat. sol. (a)* **1991,** *124* (2), 571-581.

34. Das Sarma, S.; Hwang, E. H., Universal Density Scaling of Disorder-Limited Low-Temperature Conductivity in High-Mobility Two-Dimensional Systems. *Phys Rev B* **2013,** *88* (3), 035439.
35. Cheng, C. Y.; Pai, W. L.; Chen, Y. H.; Paylaga, N. T.; Wu, P. Y.; Chen, C. W.; Liang, C. T.; Chou, F. C.; Sankar, R.; Fuhrer, M. S.; Chen, S. Y.; Wang, W. H., Phase Modulation of Self-Gating in Ionic Liquid-Functionalized Inse Field-Effect Transistors. *Nano Lett* **2022,** *22* (6), 2270-2276.
36. Iwasaki, T.; Muruganathan, M.; Schmidt, M. E.; Mizuta, H., Partial Hydrogenation Induced Interaction in a Graphene–Sio2 Interface: Irreversible Modulation of Device Characteristics. *Nanoscale* **2017,** *9* (4), 1662-1669.
37. Li, S.-L.; Wakabayashi, K.; Xu, Y.; Nakaharai, S.; Komatsu, K.; Li, W.-W.; Lin, Y.-F.; Aparecido-Ferreira, A.; Tsukagoshi, K., Thickness-Dependent Interfacial Coulomb Scattering in Atomically Thin Field-Effect Transistors. *Nano Lett.* **2013,** *13* (8), 3546-3552.
38. Cheng, H. C.; Shiue, R. J.; Tsai, C. C.; Wang, W. H.; Chen, Y. T., High-Quality Graphene P-N Junctions Via Resist-Free Fabrication and Solution-Based Noncovalent Functionalization. *Acs Nano* **2011,** *5* (3), 2051-2059.
39. Goldmann, C.; Gundlach, D. J.; Batlogg, B., Evidence of Water-Related Discrete Trap State Formation in Pentacene Single-Crystal Field-Effect Transistors. *Appl. Phys. Lett.* **2006,** *88* (6), 063501.
40. Late, D. J.; Liu, B.; Matte, H. S. S. R.; Dravid, V. P.; Rao, C. N. R., Hysteresis in Single-Layer Mos2 Field Effect Transistors. *Acs Nano* **2012,** *6* (6), 5635-5641.
41. Boutchacha, T.; Ghibaudo, G., Improved Modeling of Low-Frequency Noise in Mosfets—Focus on Surface Roughness Effect and Saturation Region. *IEEE Transactions on Electron Devices* **2011,** *58* (9), 3156-3161.
42. Chen, J.-H.; Jang, C.; Xiao, S.; Ishigami, M.; Fuhrer, M. S., Intrinsic and Extrinsic Performance Limits of Graphene Devices on Sio2. *Nat Nanotechnol* **2008,** *3* (4), 206-209.
43. You, Y. G.; Ahn, J. H.; Park, B. H.; Kwon, Y.; Campbell, E. E. B.; Jhang, S. H., Role of Remote Interfacial Phonons in the Resistivity of Graphene. *Appl Phys Lett* **2019,** *115* (4), 043104.

TOC

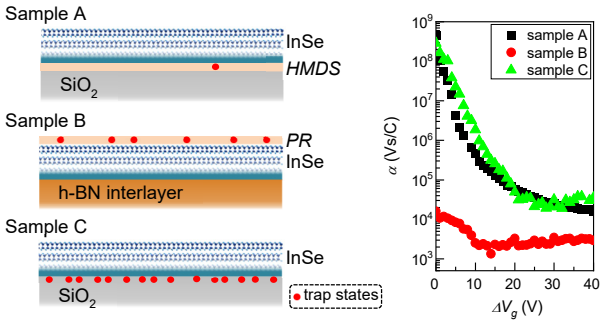
Sample A
InSe
HMDS
SiO2
Sample B
PR
InSe
h-BN interlayer
Sample C
InSe
SiO2
trap states
sample A
sample B
sample C
α (Vs/C)
ΔVg (V)